19

Plasmon-enhanced energy transfer in hybrid porous structures for luminescent sensors

© I.Yu. Nikitin, L.N Borodina, A.V. Boltenko, M.A. Baranov, P.S. Parfenov, I.A. Gladskikh, T.A. Vartanyan

ITMO University,
St. Petersburg, Russia
e-mail: nikitin0igor512@gmail.com

Received May 16, 2024
Revised September 18, 2024
Accepted September 27, 2024

A hybrid nanostructure consisting of an island silver film coated with nanoporous aluminum oxide obtained by anodic oxidation of a metallic aluminum film was synthesized and studied. In the presence of silver nanoparticles, the intrinsic luminescence of anodic aluminum oxide, caused by the presence of luminescent centers in its structure, is enhanced. Application of the Rhodamine 6G dye to the synthesized nanostructure leads to quenching of the luminescent centers of aluminum oxide with a simultaneous increase in the luminescence intensity of the dye, which indicates effective excitation transfer from the luminescent centers to the dye in the presence of silver nanoparticles with plasmon resonance in a close frequency band. The synthesized structure can find application in optical sensors and receivers of optical radiation.

Keywords: Plasmon resonance, Anodic alumina, Thin films, Luminescent sensors.

DOI: 10.61011/EOS.2024.09.60047.6675-24

Introduction

Hybrid structures, based on anodic alumina matrices and plasmonic nanoparticles are being extensively studied today, since they can be used as optical coatings, in photovoltaics, and also as substrates for *in-vitro* diagnostics of various diseases [1–3]. Major focus in the last application is made on the Raman scattering and luminescence effects [4–6]. Complex high-cost apparatus is required for Raman scattering detection. Luminescent signal is a more affordable signal to detect, but it's intensity is usually not high enough [7,8]. The existing geometries of hybrid porous structures are not suitable for luminescence enhancement, since plasmonic nanostructures in them come into direct contact with the analyte, which leads to luminescence quenching [9]. This paper describes the fabrication process and optical properties of a hybrid structure which is based on silver island film beneath a thin nanoporous matrix of aluminum oxide; this structure serves not only as a spacer preventing analyte-metal contact, but also increases the intensity of the luminescent dye on the surface and in pores of the hybrid structure due to a resonance energy transfer from its luminescent centers[10–12].

Materials and methods

Silver and aluminum sputtering

In this study the hybrid porous structure, as well as nanoporous anodic alumina matrices were fabricated in several stages. Prior to sputtering, the glass substrates $26 \times 76\,mm^2$ in size were cleaned using isopropyl alcohol and deionized water. After that, the substrates were placed for 30 min in „piranha solution" ($H_2O_2 : 3H_2SO_4$) for removal of organic impurities. After having soaked in the mixture, all substrates were cleaned with a large amount of deionized water, wiped dry and purged with nitrogen to remove the dust particles. The samples were then placed in a vacuum unit for physical vapor-phase deposition (Kurt J. Lesker, USA), where first silver was spluttered on them, and after silver annealing — aluminum. With every sputtering the chamber was pumped out to obtain vacuum of 10^{-6} Torr. Silver was sputtered using resistive heating of a tungsten boat, aluminum — using electron beam evaporation. Thickness and speed were monitored during each sputtering using the resonance frequency method.

The thickness of silver film was 15 nm at a sputtering rate of 0.3 Å/s. After sputtering the silver films were annealed in the air to obtain an island-like structure where a localized plasmonic resonance was observed [13]. The silver films were annealed at a temperature of 250°C, controlled by a thermocouple.

After annealing the aluminum films 160 nm thick were deposited above. When sputtering aluminum, the same vacuum regime was observed as when sputtering the silver. The sputtering rate was 0.6 Å/s. Further, the films were subjected to anodizing.

Anodizing of aluminum

Anodizing is a complex electrochemical process, as a result of which the thickness of the oxide film appearing on aluminum surface in natural conditions can be increased. Depending on the electrolyte and current density in the electrochemical cell, the appearing oxide

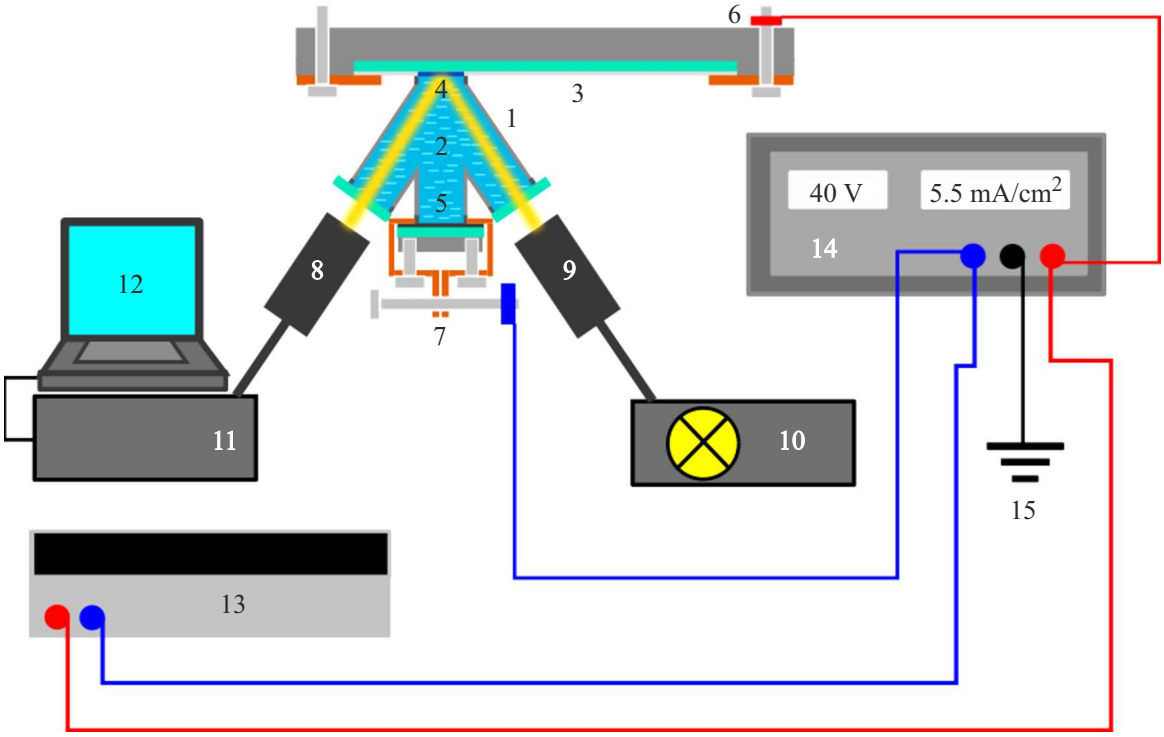

Figure 1. Schematic representation of an electrochemical cell with a spectrum control: *1* — cell body with insulation gaskets; *2* — working space filled with electrolyte; *3* — sample; *4* — anodized area of the sample; *5* — graphite cathode; *6* — copper electrode; *7* — cathode; *8* — detector; *9* — fiber-optic output of lamp; *10* — lamp; *11* — spectrometer unit; *12* — PC; *13* — laboratory multimeter; *14* — laboratory power unit; *15* — earthing.

film may have greater or lesser porosity, and under certain conditions the pores may form regular structures. The thin-film anodizing unit is shown in Fig. 1. This unit is distinguished by the fact that anodizing process in it can be controlled by method of reflectometry. During the process of thin-film anodizing in 0.3 M oxalic acid at voltage of 40 V and current density of 5.5 mA/cm^2 the reflectance spectra are registered every 5 s. The spectra are recorded using a fiber multichannel spectrometer PMA-12 (Hamamatsu, Japan). Voltage is controlled by multimeter ABM-4403 (Aktakom-Iwatsu, Japan).

During anodizing process electrolyte is used at various temperatures. Electrolyte temperature in case from 0°C to 5°C is maintained using an ice bath, in other cases using a furnace with a built-in thermocouple. Several temperature modes were used during anodizing: 0−5°C and 40°C.

Reflectance spectra were recorded before, during, and after anodizing of hybrid porous structures and anodic alumina. Diffusive and full reflectance spectra were obtained before and after anodizing. Both types of spectra were recorded using an integrating sphere SF-56 (LOMO Spektr, Russia). The luminescence spectra were recorded using the scanning laser con-focal microscope LSM710 (Zeiss, Germany). The luminescence kinetics was registered using the correlated photon counting technique on the confocal time-resolved photoluminescence microscope MicroTime100 (PicoQuant, Germany) The relief of the structure was studied using the scanning electron microscope Merlin (Zeiss, Germany) and the atomic force microscope Solver PRO-M (NT-MDT Russia).

Application of coating

Rhodamine 6J was selected as a dye since its optical properties are described in a large number of papers. The dye was introduced by impregnating aluminum oxide on both, glass plate and silver nanoparticles with an ethanol solution of rhodamine 6J with a concentration of $2 \cdot 10^{-4}$ M at 60°C in 24h. The luminescence spectra and decay kinetics were recorded both, before and after impregnation.

Results and discussion

Structure

Images of silver island film, hybrid structure and thin aluminum film before anodizing, obtained using the scanning electron microscope are shown in Fig. 2.

The following is presented in the images: an array of nanoparticles shown in white, an array of nanoparticles under an aluminum film shown in light gray, as well as the relief of an aluminum film deposited on a slide. The

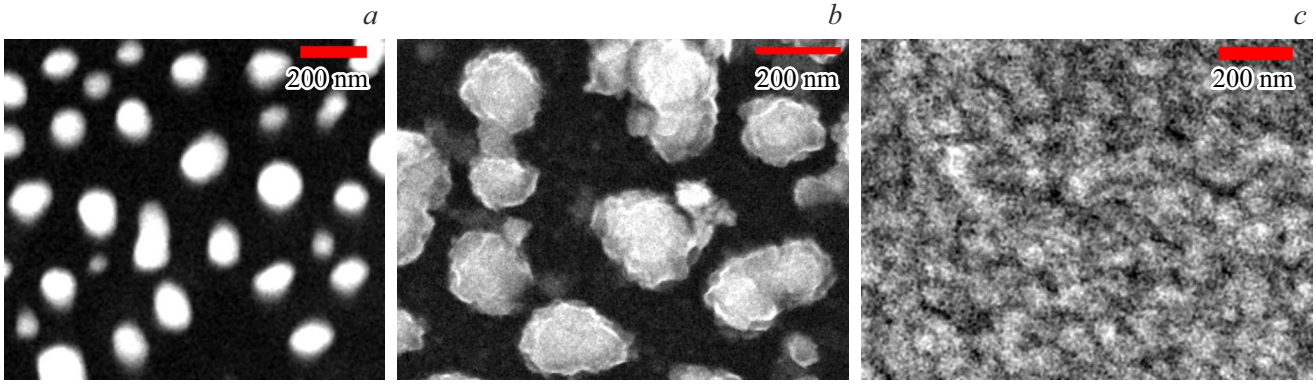

Figure 2. Images of silver island-like film (a), hybrid structure (b) and thin aluminum film before anodizing (c), obtained using scanning electron microscopy.

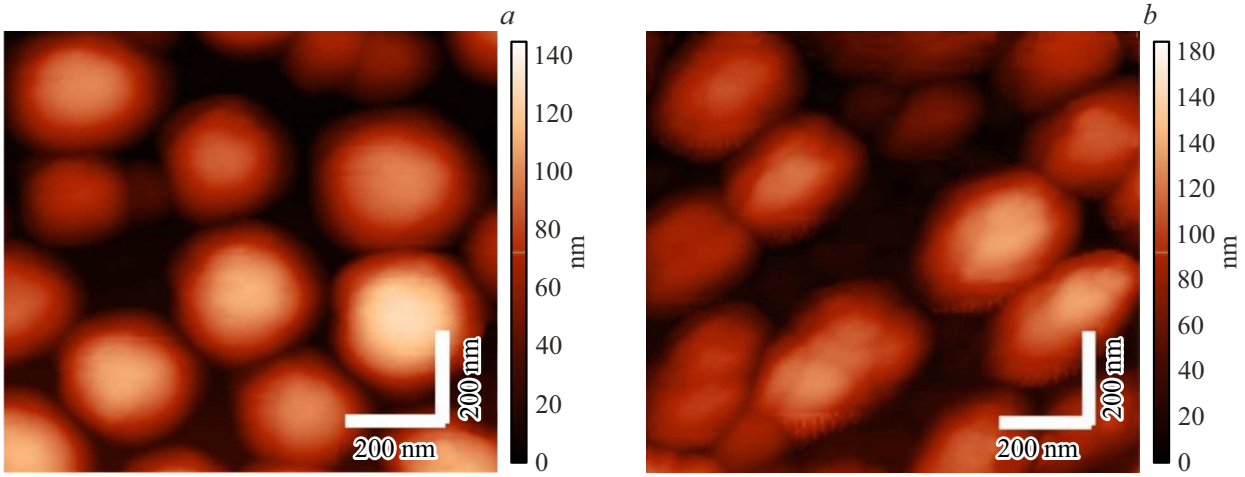

Figure 3. Topographic images of plasmonic nanoparticles (a) and hybrid structure before anodizing (b), obtained with the use of atomic-force microscopy.

brighter the area in the image, the larger is the amount of sample-scattered secondary electrons that reach the detector.

The images of structures, obtained using the atomic-force microscope are shown in Fig. 3.

The image shows an array of plasmonic silver nanoparticles in the air and beneath an aluminum film, respectively. The height in the images is denoted by color.

AFM-images are well correlated with the SEM-images. For the hybrid structure, an inhomogeneous structure of nanoparticles is also observed after aluminum deposition.

The images obtained on a scanning electron microscope after anodizing thin films of aluminum and hybrid structures are shown in Fig. 4.

Image of the anodized hybrid porous structure obtained with the use of the atomic force microscope is given in Fig 5.

Silver nanoparticles (Fig 2, a) form white areas with lateral sizes of about 100 nm. These particles form a surface relief which stays unchanged after the aluminum film is deposited on it (Fig. 2, b). The particles structure becomes more of a grain type, similar to the aluminum film (Fig. 2, c).

The white areas represent the relief, as in the images obtained with the atomic force microscope, a similar pattern is observed in the form of protruding areas shown in a lighter tone. At that, the effect of dielectric surface charging due to bombardment by electrons is excluded.

The porous structure of anodic aluminum oxide is visible in almost all images of the anodized samples. The white zones represent the relief and have the same height as before anodizing, as shown in the corresponding AFM image.

AFM-image in Fig. 5 proves that white spots on SEM-images designate the structure relief.

Reflection

By subtracting the diffuse reflectance spectra from the total reflectance spectra, specular reflectance spectra similar to those recorded during anodizing can be obtained. Total and diffuse reflectance spectra of the hybrid structure and aluminum film before anodization compared to the spectra of plasmonic nanoparticles are shown in Fig. 6.

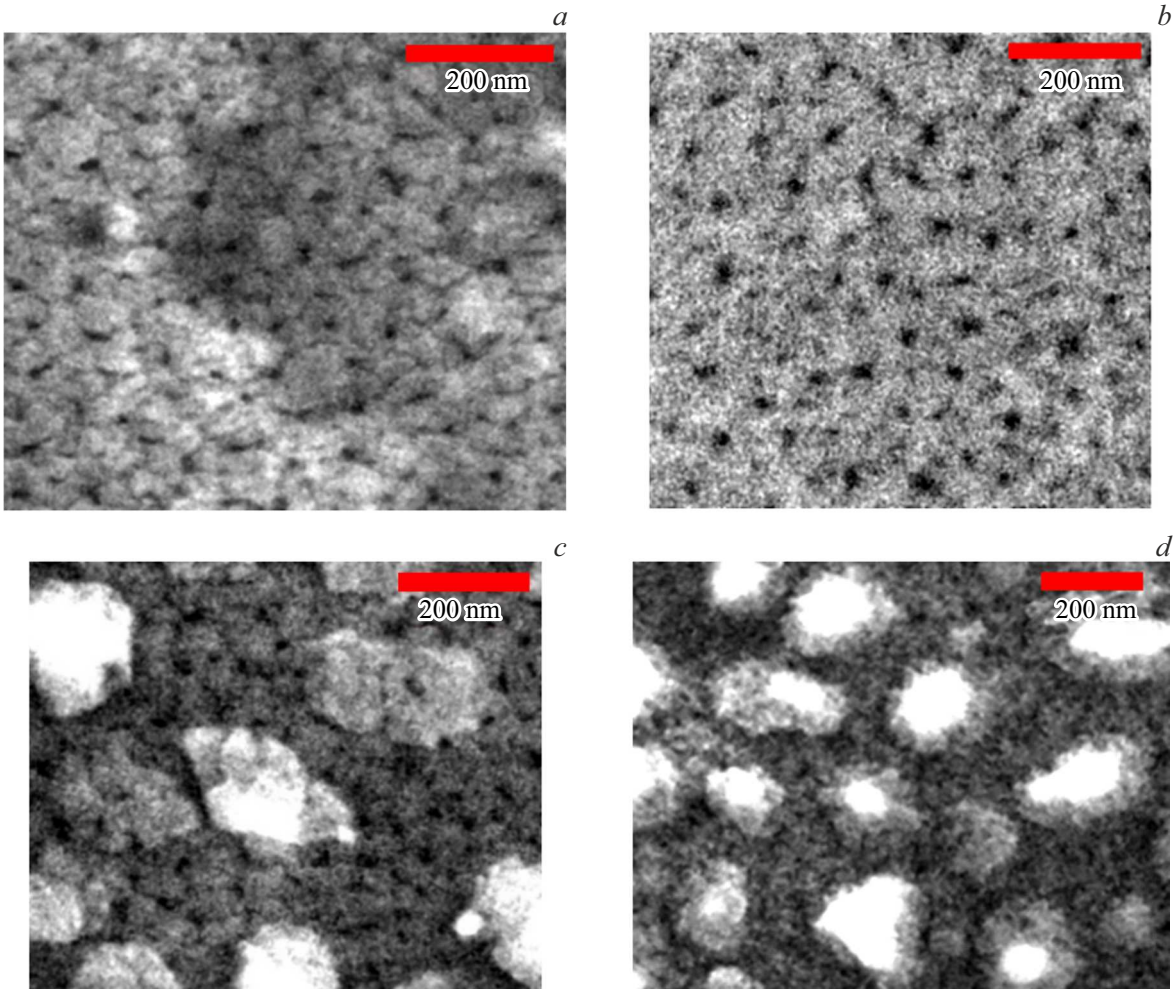

Figure 4. Images of aluminum oxide anodized at 5°C (*a*) and at 40°C (*b*), as well as images of hybrid porous structure anodized at 5°C (*c*) and at 40°C (*d*) obtained with the use of scanning electron microscope.

The Figure illustrates total, diffuse, and specular reflectance spectra of a silver island film, aluminum film, and an island film beneath the aluminum film. Total reflectance spectrum is a sum of specular and diffuse reflectance spectra.

Specular reflectance spectra obtained during anodizing on a multichannel spectrometer PMA-12 (Hamamatsu, Japan), are shown in Fig. 7.

The figure shows the reflectance spectra of anodic aluminum oxide recorded during anodizing. The color code indicates the time of spectrum registration, counted from the beginning of the process. This time is shown on a separate scale near each curve. In all cases, a sample of thin aluminum film before anodizing was used as a reference sample.

The reflectance spectra (Fig. 8) are recorded and presented similarly to the reflectance spectra before anodizing the samples.

In the silver reflectance spectra (Fig. 6), a band with a maximum at 500 nm is observed, corresponding to the plasmonic resonance of the structure. The band is observed in both, the specular reflectance, total and diffuse reflectance spectra of the particles, which is typical for coarse particles [14]. The minimum in the total reflectance spectrum at 850 nm corresponds to the intrinsic optical characteristics of aluminum [15]. The hybrid structure has a minimum at about 300 nm, in the blue region of specular reflectance spectra, possibly due to Rayleigh scattering on irregularities generated by nanoparticles beneath the aluminum layer.

In the reflectance spectra obtained in the anodizing process at various electrolyte temperatures (Fig. 7), some differences are observed in the endpoint mean reflectance for the anodized films. This can be explained by the balance of films oxidation and dissolution reactions. These reactions affect the porosity of films, and, as a consequence — the refractive index of nano-porous alumina, and consequently, its reflectance spectrum. At a higher temperature of the electrolyte, the reflection of the oxide film changes faster, which is associated with an increase in the rates of oxidation

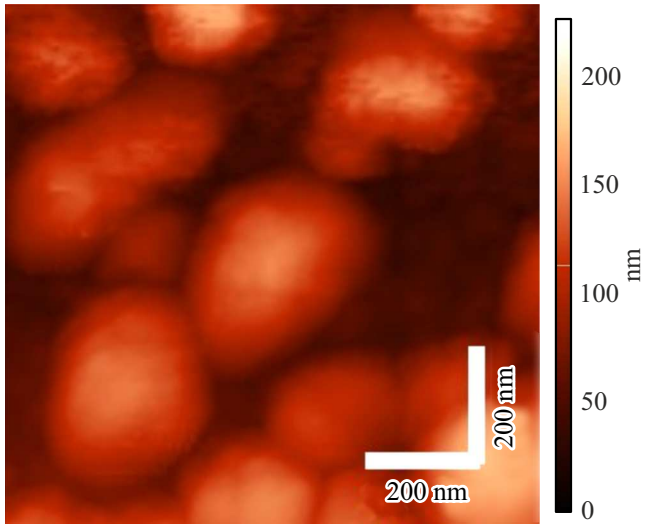

Figure 5. Topographic images of a hybrid structure anodized at 40°C, obtained with the use of atomic-force microscopy.

and dissolution of the oxide. The same patterns are observed for thick aluminum oxide films anodized in aluminum foil [16].

The reflectance spectra of anodic aluminum oxide films obtained after anodizing (Fig. 8) for both electrolyte temperatures look similarly, which may indicate that the aluminum film was completely anodized at both temperatures. For hybrid structures, anodizing at various temperatures gives different reflectance spectra, the shape of which is provided by the differences between the total and diffuse reflectance spectra. In case of anodizing at lower temperatures, a plasmon maximum is observed in the total reflectance spectrum of the hybrid porous structure, and the diffuse reflection looks similar to the diffuse reflection of aluminum oxide. At higher anodizing temperatures, on the contrary, the total reflectance spectrum resembles the spectrum of aluminum oxide in shape, while the plasmon maximum is visible in the diffuse reflectance spectrum. When subtracting the diffuse reflectance spectra from the total reflectance spectra, we may see a maximum in the reflectance in the first case and a minimum at a wavelength of the plasmonic resonance maximum. Since in both cases the optical characteristics of aluminum oxide without nanoparticles differ from each other insufficiently, it is assumed that plasmonic nanoparticles beneath the matrix have an effect on the specular reflectance and diffuse reflectance spectra. To determine the nature of the effect, it is necessary to consider the temperature dependence of the reflectance spectra in a more detailed way. For this, additional study is required.

Luminescence

The luminescence spectra of aluminum oxide and hybrid porous structures obtained using the laser scanning confocal microscope LSM710 (Zeiss, Germany) are shown in Fig. 9.

The luminescence spectra presented on the figure were recorded under the same conditions and at the same power of the excited light. Luminescence of aluminum oxide if anodized at a temperature of 40°C has higher intensity compared to the luminescence of oxide anodized at a temperature of 5°C. This may be due to the formation of a larger amount of luminescent centers, defects in the oxide lattice, as well as carboxyl groups oriented onto aluminum atoms during the anodizing process [17,18]. Luminescent centers can act as energy donors for luminescent dyes [19]. The long-wavelength shift of the luminescence maximum of the dye in the oxide matrix compared to the dye on the glass, as well as the appearance of the second maximum, may be caused by the aggregation of the dye on the surface of aluminum oxide, since the dye has quite high concentration here. Alumina in hybrid structures has higher luminescence intensity. This intensification occurs due to the Purcell effect when plasmonic nanoparticles interact with the luminescent centers of anodic alumina, which leads to an increase in the intensity of alumina luminescence, as well as reduces its decay time, as shown in the next section.

Luminescence decay time

Sample	Decay time, ns
Ag/Al_2O_3 5°C	18.9 ± 0.1
Al_2O_3 5°C	19.6 ± 0.1
Ag/Al_2O_3 40°C	16.9 ± 0.1
Al_2O_3 40°C	20.3 ± 0.1

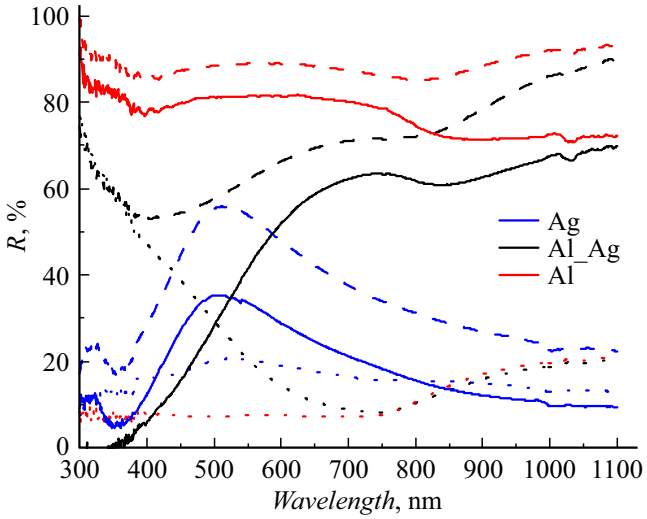

Figure 6. Spectra of specular reflectance (solid line), total reflectance (dashed line) and diffuse reflectance (dotted line) of plasmonic nanoparticles (blue), as well as aluminum films (red) and hybrid structures before anodizing (black).

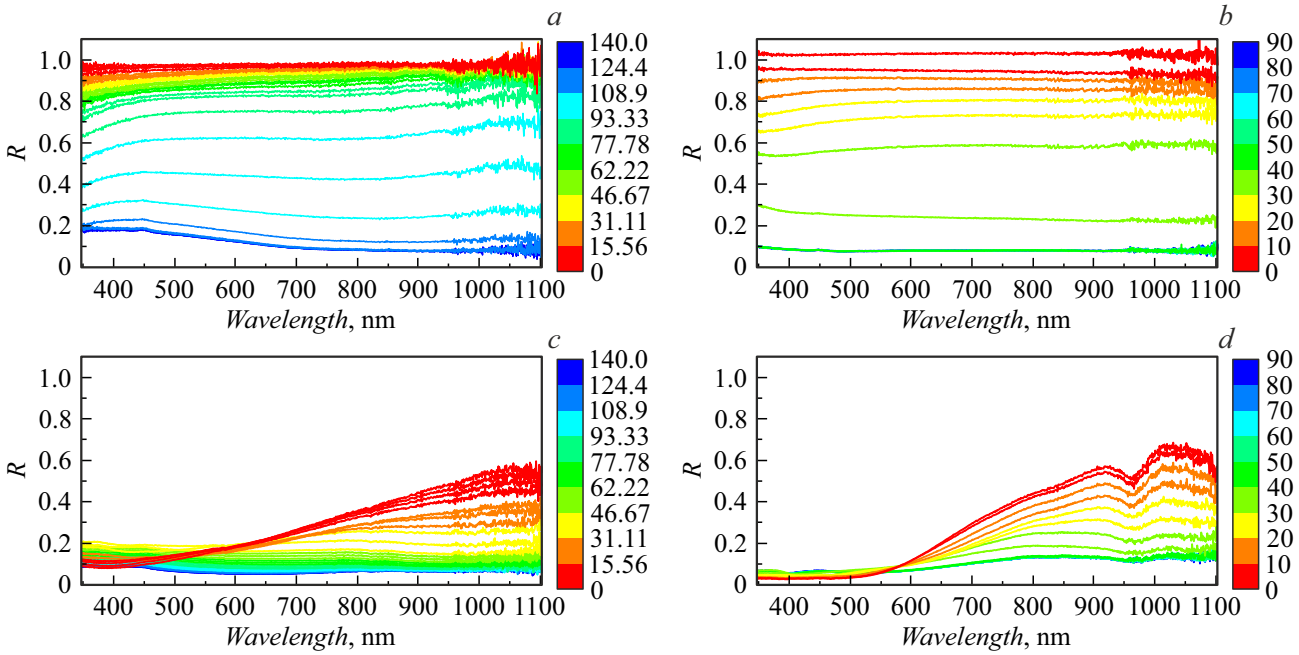

Figure 7. Specular reflectance spectra of aluminum anodized at 5°C (*a*) and at 40°C (*b*), as well as spectra of hybrid porous structure anodized at 5°C (*c*) and at 40°C (*d*), obtained using the multichannel spectrometer every 5 s. The anodizing time in seconds is indicated by the color code in the columns to the right of the graphs.

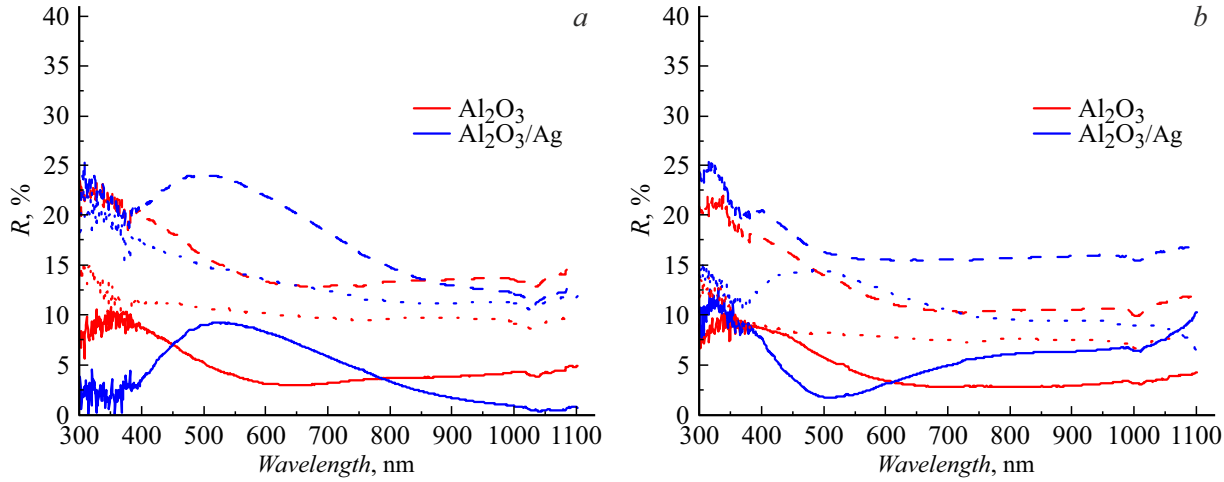

Figure 8. Specular reflectance (solid line), total reflectance (dashed line), and diffuse reflectance (dotted line) spectra of aluminum oxide films (red) and hybrid porous structures (blue) anodized at 5°C (*a*) and at 40°C (*b*).

Luminescence kinetics

Figure 10 shows the luminescence decay kinetics for samples anodized in two temperature modes; the kinetics was obtained using Confocal time-resolved photoluminescence microscope MicroTime100 (PicoQuant, Germany).

The kinetics of luminescence decay is normalized and presented on a logarithmic scale in order to make it easier to compare the decay kinetics for different samples. The table below shows the average lifetime of excited states for various samples, calculated by formula:

$$\tau_{av} = \frac{\int_0^{\tau_{\max}} t^2 f(t)dt}{\int_0^{\tau_{\max}} t f(t)dt}.$$

At lower temperatures of the electrolyte the luminescence decay of anodic alumina, on the glass and in the hybrid porous structure takes more time. This may occur due to lesser amount of luminescent centers in the structure where the charge carriers may have radiative recombination. In the

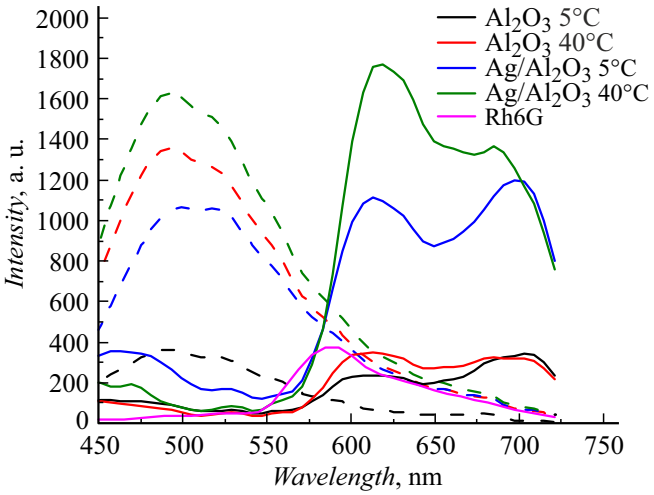

Figure 9. Luminescence spectra of aluminum oxide (black and red), as well as of the hybrid porous structure (blue and green) with and without dye (solid line) (dashed line), as well as the luminescence spectrum of rhodamine 6J on glass (pink). The excitation wavelength is 405 nm. Objective lens: Zeiss FLUAR 20x 0.75NA. Power density 8.31 mW/cm^2.

presence of plasmonic nanoparticles, the lifetime of the excited state in anodic alumina decreases possibly caused by Purcell effect that occurs when plasmonic nanoparticles interact with the luminescent centers of anodic aluminum oxide. The short lifetime of the excited state under intense luminescence indicates a high probability of a radiative transition in the sample. An increase in the probability of a radiative transition may occur due to the influence of an external electromagnetic field on the radiating system, which in this case may occur near a plasmonic nanoparticle. When particles absorption spectra and luminescence spectra of aluminum oxide are overlapped, a positive feedback may occur, leading to an increase in the luminescence intensity of the entire system. Due to this effect, there is an increase in the luminescence intensity of aluminum oxide in the hybrid porous structure, as shown in Fig. 9.

Conclusions

The morphology and optical properties of the hybrid structure based on silver plasmon nanoparticles and aluminum oxide, as well as anodic alumina films individually, were analyzed in the study.

1. The nature of the images of the hybrid structure before and after anodizing is determined by the relief created by nanoparticles located at the base of this structure, which was found by comparing AFM and SEM images.

2. In the reflectance spectra recorded before anodizing, the minimum of about 850 nm in the aluminum reflectance spectrum is due to the intrinsic optical properties of aluminum, and the minimum in 300 nm region is due to Rayleigh scattering on the relief generated by silver nanoparticles in the film base.

3. The reflectance spectra obtained during anodizing show an increase in the rate of reflectance decrease at higher temperatures of the electrolyte, which may mean an increase in the speed of the process itself. This is due to the oxidation and dissolution reactions of aluminum oxide, the rate of which depends, among other things, on temperature, and in this case thin films of aluminum oxide are no different from those obtained by anodizing thick layers of aluminum [16].

4. There is no significant qualitative difference in the reflectance spectra recorded after anodizing of anodic alumina. That is why the qualitative differences in the reflectance spectra of hybrid structures can most likely be due to the anodizing process effect on plasmonic nanoparticles. Additional studies are required to determine the nature of this effect.

5. The patterns described below are observed in the spectra of luminescence hybrid structures with and without use of the dye. When a dye is added to aluminum oxide,

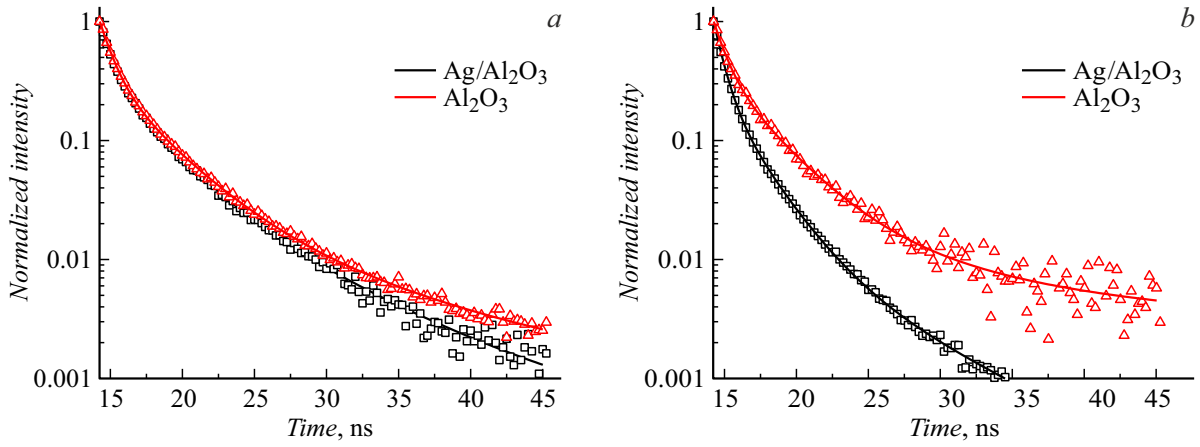

Figure 10. Kinetics of luminescence decay of anodic alumina (red), as well as of hybrid porous structures (black) during anodizing in electrolyte at a temperature of5°C (*a*) and 40°C (*b*). Solid lines indicate approximating curves based on three-exponential functions. The excitation wavelength is 405 nm. Objective lens: Olympus 40x 0.65NA. Power density 49 mW/cm^2.

both in the structure and on the glass, the luminescence of aluminum oxide is extinguished and that of the dye goes high. This may be caused by the resonant energy transfer from the luminescent centers formed in the oxide during anodization to the dye, its molecules and aggregates. The dye may have aggregated in the pores and on the surface of the oxide, since, compared to the dye spectra on the glass, a long-wavelength shift of the luminescence maximum and the formation of a second maximum are observed in aluminum oxide and in the hybrid structure. Compared to aluminum oxide, the hybrid structure has a more intense luminescence, which may be due to the Purcell effect, which manifests itself during interactions between luminescent centers in aluminum oxide and plasmonic nanoparticles in the base of the hybrid structure.

6. Purcell effect in the structure is proved by the samples luminescence kinetics. In the presence of plasmonic nanoparticles, the luminescence lifetime of anodic alumina decreases, which may be associated with an increased probability of the radiative transition in luminescent centers.

The observed regularities may be used for fabrication of luminescent sensors used in the optical sensors and radiation detectors.

Acknowledgments

The authors express their thanks to A.V. Veniaminov for the valuable remarks made during the study.

Funding

This study was supported by the Russian Science Foundation, grant № 23-72-00045, https://rscf.ru/project/23-72-00045/

Conflict of interest

The authors declare that they have no conflict of interest.

References

[1] T. Kondo, T. Sano, T. Yanagishita, H. Masuda, J. Phys. Chem. C, **127** (44), 21629 (2023). DOI: 10.1021/acs.jpcc.3c05264
[2] U. Malinovskis, R. Poplausks, D. Erts, K. Ramser, S. Tamulevičius, A. Tamulevičienė, Y. Gu, J. Prikulis, Nanomaterials, **9** (4), 531 (2019). DOI: 10.3390/nano9040531
[3] W.J. Ho, P.Y. Cheng, K.Y. Hsiao, Appl. Surf. Sci., **354**, 25 (2015). DOI: 10.1016/j.apsusc.2015.05.049
[4] O. Stranik, H.M. McEvoy, C. McDonagh, B.D. MacCraith, Sensors Actuators, B Chem., **107** (1 spec. iss.), 148 (2005). DOI: 10.1016/j.snb.2004.08.032
[5] I.Y. Nikitin, K.A. Maleeva, D. Kafeeva, A.V. Nashyokin, I.A. Gladskikh. In: *Proc. of SPIE/COS Photonics Asia 2023* (SPIE, 2023), vol. 12774, p. 12774D-1, DOI: 10.1117/12.2686292
[6] N.T.T. Phuong, T.A. Nguyen, V.T. Huong, L.H. Tho, D.T. Anh, H.K.T. Ta, T.H. Huy, K.T.L. Trinh, N.H.T. Tran, Micromachines, **13** (11), 1840 (2022). DOI: 10.3390/mi13111840
[7] A.B. Taylor, P. Zijlstra, ACS Sensors, **2** (8), 1103 (2017). DOI: 10.1021/acssensors.7b00382
[8] G. Sun, J.B. Khurgin, IEEE J. Sel. Top. Quantum Electron., **17** (1), 110 (2011). DOI: 10.1109/JSTQE.2010.2047249
[9] C.R. Simovski, M.S.M. Mollaei, P.M. Voroshilov. Phys. Rev. B, **101** (24), 245421 (2020). DOI: 10.1103/PhysRevB.101.245421
[10] F. Reil, U. Hohenester, J.R. Krenn, A. Leitner, Nano Lett., **8** (12), 4128 (2008). DOI: 10.1021/nl801480m
[11] A. Mohammadpour, I. Utkin, S.C. Bodepudi, P. Kar, R. Fedosejevs, S. Pramanik, K. Shankar, J. Nanosci. Nanotechnol., **13** (4), 2647 (2013). DOI: 10.1166/jnn.2013.7348
[12] R.D. Nabiullina, I.Y. Nikitin, E.O. Soloveva, I.A. Gladskikh, A.A. Starovoytov. In: *Proc. of SPIE Photonics Europe 2022*, ed. by D.L. Andrews, A.J. Bain, J.-M. Nunzi (SPIE, Strasbourg, 2022), p. 6. DOI: https://doi.org/10.1117/12.2621343
[13] N.A. Toropov, I.A. Gladskikh, P.S. Parfenov, T.A. Vartanyan, Opt. Quantum Electron., **49** (154), 1 (2017). DOI: 10.1007/s11082-017-0996-5
[14] V. Klimov, Nanoplazmonika, 2-d ed. (Fizmatlit, M., 2010) (in Russian).
[15] F. Cheng, P.H. Su, J. Choi, S. Gwo, X. Li, C.K. Shih, ACS Nano, **10** (11), 9852 (2016). DOI: 10.1021/acsnano.6b05556
[16] R.A. Mirzoev, A.D. Davidov, *Anodnie protsessi elektrokhimicheskoy obrabotki metallov*, 4-th ed. (Lan', SPb, M., Krasnodar, 2022) (in Russian).
[17] Y. Yamamoto, N. Baba, S. Tajima, Nature, **289**, 572 (1981).
[18] Y. Du, W.L. Cai, C.M. Mo, J. Chen, L.D. Zhang, X.G. Zhu, Appl. Phys. Lett., **74** (20), 2951 (1999). DOI: 10.1063/1.123976
[19] A. Makhal, S. Sarkar, S.K. Pal, H. Yan, D. Wulferding, F. Cetin, P. Lemmens, Nanotechnology, **23** (30), 305705 (2012). DOI: 10.1088/0957-4484/23/30/305705

Translated by T.Zorina